First-principles DFT + *GW* study of oxygen-doped CdTe

Mauricio A. Flores,[1,*] Walter Orellana,[2] and Eduardo Menéndez-Proupin[1]

[1]*Departamento de Física, Facultad de Ciencias, Universidad de Chile, Las Palmeras 3425, 780-0003 Ñuñoa, Santiago, Chile*

[2]*Departamento de Ciencias Físicas, Universidad Andres Bello, República 220, 037-0134 Santiago, Chile*

(Received 1 December 2015; revised manuscript received 17 March 2016; published 16 May 2016)

The role of oxygen doping in CdTe is addressed by first-principles calculations. Formation energies, charge transition levels, and quasiparticle defect states are calculated within the DFT + *GW* formalism. The formation of a new defect is identified, the (O_{Te}-Te_{Cd}) complex. This complex is energetically favored over both isovalent (O_{Te}) and interstitial oxygen (O_i), in the Te-rich limit. We find that the incorporation of oxygen passivates the harmful deep energy levels associated with (Te_{Cd}), suggesting an improvement in the efficiency of CdTe based solar cells. Substitutional (O_{Cd}) is only stable in the neutral charge state and undergoes a Jahn–Teller distortion. We also investigate the diffusion profiles of interstitial oxygen and find a low-energy diffusion barrier of only 0.14 eV between two structurally distinct interstitial sites.

DOI: 10.1103/PhysRevB.93.184103

I. INTRODUCTION

CdTe is one of the few II-VI semiconductors that can be doped both *n* and *p* type [1–4]. Due to their high atomic number, large band gap, and good mobility-lifetime product, CdTe and its alloys have become of great importance in a wide range of applications including photovoltaics, room-temperature x-ray and gamma-ray detection applications, medical imaging, industrial process monitoring, nondestructive testing, and nuclear safeguards [5–7]. Applications in x-ray and gamma-ray radiation detectors require a material with high resistivity ($>10^9$ Ω cm) and a low concentration of carrier traps. It is well known that high resistivity in CdTe is achieved through the pinning of the Fermi-level near midgap by compensation through a balance between shallow- and deep-level defects [8,9]. Among photovoltaics, CdTe is one of the most promising materials due its near-optimum band gap of $\sim$1.5 eV, high absorption coefficient, and low manufacturing cost [10–14].

The dominant intrinsic defect in CdTe is believed to be the Cd vacancy (V_{Cd}), which behaves as a dominant acceptor [15]. This defect is responsible for the *p*-type conductivity undoped CdTe [16,17]. To compensate the excess holes, shallow donors such as In, Al, or Cl, and IV-group deep donors such as Ge and Sn have been suggested [18–20]. However, a precise balance between shallow acceptors and shallow donors is not possible in practice. It is widely believed that the high resistivity of undoped CdTe is due to a deep donor level induced by a native defect. This donor is usually assumed to be a Te antisite (Te_{Cd}) [21–24]. However, several theoretical results show that (Te_{Cd}) induces a gap level that is too shallow to pin the Fermi level close to the midgap [16,22,25]. Recent theoretical and experimental results suggest that some deep levels may also be induced by dislocations [26,27].

Most of CdTe crystals are grown by conventional Bridgman and high-pressure Bridgman techniques, resulting in a Te-rich material with a high concentration of Cd vacancies and Te antisites. Moreover, mass spectroscopy measurements show that residual oxygen has a concentration typically orders of magnitudes higher than other residual impurities and comparable to intrinsic defects [28]. The presence of oxygen changes the physical properties of CdTe thin films, especially its electrical resistivity [29]. Oxygen can increase the open circuit voltage from 780 to 812 mV in CdS/CdTe thin-film solar cells [30–32]. However, at high concentration, oxygen can increase the resistivity of the device, probably due to the generation of nonradiative defects [33]. Valdna [34] has shown that the incorporation of a small quantity of oxygen decreases the resistivity of CdTe:Cl films, whereas at higher concentration oxygen is assumed to form isoelectronic complexes with cadmium vacancies, leading to a sharp increase in the resistivity. Furthermore, Hsu and coworkers [35] have pointed out that oxygen impurities do not behave as shallow acceptors but as isoelectronic traps forming complexes based on cadmium vacancies.

In this paper we investigate the role of oxygen doping in CdTe. Interstitial (O_i), isovalent (O_{Te}), substitutional (O_{Cd}), and the complexes (V_{Cd}-O_{Te}) and (O_{Te}-Te_{Cd}) are studied within the DFT + *GW* formalism [36–38], which combines DFT total energy and many-body *GW* quasiparticle calculations. Our results suggest a beneficial effect of oxygen in the passivation of nonradiative recombination centers associated with (Te_{Cd}), thereby improving the efficiency of CdTe based solar cells.

II. METHODS

A. Computational methods

First-principles total-energy and band-structure calculations were performed by using density functional theory and the generalized gradient approximation functional of Perdew, Burke, and Ernzerhof (PBE) [39] as implemented in the QUANTUM-ESPRESSO package [40]. Electron-ion interactions were described by GBRV ultrasoft pseudopotentials [41]. To avoid finite-size effects as much as possible, the defect calculations were performed within a large 512-atom cubic supercell. The valence wave functions were expanded in a plane-wave basis with a cutoff energy of 390 eV. Increasing the cutoff energy up to 490 eV changes the formation energies of neutral defects by only 0.03 eV. Therefore, considering

*mauricio.flores@ug.uchile.cl

the computational demand of the supercell calculations, the lowest cutoff was selected. All the atoms were fully relaxed until the forces on every atom where less than 0.025 eV/Å. The Brillouin zone integration was sampled with the Γ point only.

Many-body G_0W_0 calculations with defect supercells were performed using the WEST code [42,43], which avoids an explicit sum over empty orbitals by using a technique called projective eigendecomposition of the dielectric screening (PDEP) [42] and evaluates the correlation self-energy by a Lanczos-chain algorithm [44]. We used 200 projective dielectric eigenpotential basis vectors to represent the dielectric matrix and 30 Lanczos steps for evaluating the irreducible polarizability, which is sufficient to obtain a well-converged band gap within 0.1 eV. For the absolute position of the valence band maximum (VBM) we used $\Delta E_{\mathrm{VBM}} = -0.74$ eV as obtained in Ref. [45] employing the $GW\Gamma^1$ approximation. Optimized norm-conserving Vanderbilt pseudopotentials (ONCV) [46] with 20 and 16 valence electrons for Cd and Te atoms, respectively, and a plane-wave energy cutoff of 70 Ry were employed. A considerable improvement was obtained by using ONCV pseudopotentials, because the plane-wave-cutoff requirements with semicore states are modest compared to the conventional Kleinman–Bylander [47] representation. When the reference state is an open-shell system, we used wave functions and energies from spin-polarized DFT calculations as mean-field starting points for G_0W_0. The quasiparticle gap of bulk CdTe is calculated to be 1.56 eV, in good agreement with the experimental value of 1.6 eV.

B. Defect-formation energies

The formation energy of a defect in charge state q can be expressed as [48]

$$E_q^f[\mathbf{R}] = E_q[\mathbf{R}] - E_{\mathrm{ref}} + qE_F, \tag{1}$$

$$E_{\mathrm{ref}} \equiv E_{\mathrm{bulk}} + \sum_i n_i\mu_i, \tag{2}$$

where $E_q[\mathbf{R}]$ is the total energy of the system in charge state q and atomic positions $\mathbf{R}$, and E_{ref} is the energy of a reference system with the same number of atoms as the defect system. The thermodynamic formation energy is obtained when ionic positions correspond to the minimum-energy configuration for the charge state q, i.e., $\mathbf{R} = \mathbf{R}_q$. The integer n_i indicates the number of atoms of type i that have been added ($n_i > 0$) or removed ($n_i < 0$) from the supercell, and μ_i are the corresponding chemical potentials of these species. E_F is the electron chemical potential or the Fermi energy. The position of the bulk VBM with respect to the defect supercell was obtained through the alignment of the averaged electrostatic potential in a bulk-like region of the defect supercell [49].

C. Chemical potentials

The chemical potential μ_i for the ith atomic species can be written as

$$\mu_i = \mu_i^{\mathrm{ref}} + \Delta\mu_i, \tag{3}$$

where μ_i^{ref} is the chemical potential of species i in its reference phase, and $\Delta\mu_i$ is a relative chemical potential referenced to μ_i^{ref}. If the system is under thermodynamic equilibrium and there is no Te or Cd precipitation, then

$$\Delta\mu_{\mathrm{Cd}} + \Delta\mu_{\mathrm{Te}} = E^f[\mathrm{CdTe}], \tag{4}$$

where $E^f[\mathrm{CdTe}]$ is the formation energy of CdTe, which is calculated to be -0.91 eV, in good agreement with the experimental value of -0.96 eV [50]. The stability condition for CdTe requires $E^f[\mathrm{CdTe}] < \Delta\mu_{\mathrm{Te}} < 0$, and $E^f[\mathrm{CdTe}] < \Delta\mu_{\mathrm{Cd}} < 0$.

In order to put reasonable limits on the chemical potentials of oxygen impurities, we followed the work of Diehl and Noläng [51] to set thermodynamic restrictions that prevent the formation of bulk phases with the host atoms into oxides. According to their work, it is the cadmium activity in the system which determines the nature of the oxide formed. At higher values of μ_{Cd}, CdTe reacts with oxygen in the gas phase to form CdO, and at lower values of μ_{Cd}, the reaction yields $CdTeO_3$. Therefore, the relative chemical potential $\Delta\mu_{\mathrm{O}}$ is restricted by

$$\Delta\mu_{\mathrm{Cd}} + \Delta\mu_{\mathrm{Te}} + 3\Delta\mu_{\mathrm{O}} \leqslant E^f[\mathrm{CdTeO_3}], \tag{5}$$

and

$$\Delta\mu_{\mathrm{Cd}} + \Delta\mu_{\mathrm{O}} \leqslant E^f[\mathrm{CdO}]. \tag{6}$$

Here, $E^f[\mathrm{CdTeO_3}]$ is the formation energy of $CdTeO_3$ [52], which we found to be -6.54 eV. In the case of CdO, we found $E^f[\mathrm{CdO}] = -2.56$ eV, which is in good agreement with the experimental value of -2.68 eV [50].

Inserting Eq. (4) into Eq. (5), we have

$$E^f[\mathrm{CdTe}] + 3\Delta\mu_O \leqslant E^f[\mathrm{CdTeO_3}]. \tag{7}$$

Therefore, the following relation is always satisfied:

$$\Delta\mu_O \leqslant \tfrac{1}{3}(E^f[\mathrm{CdTeO_3}] - E^f[\mathrm{CdTe}]) = -1.88\ \mathrm{eV}. \tag{8}$$

From Eq. (6) we have

$$\Delta\mu_O \leqslant E^f[\mathrm{CdO}] - \Delta\mu_{\mathrm{Cd}}. \tag{9}$$

In the Cd-rich condition $\Delta\mu_{\mathrm{Cd}} = 0$, then

$$\Delta\mu_{\mathrm{O}}^{\text{Cd-rich}} \leqslant E^f[\mathrm{CdO}] = -2.56\ \mathrm{eV}. \tag{10}$$

Relation (10) is stricter than relation (8), so

$$\Delta\mu_{\mathrm{O}}^{\text{Cd-rich}} \leqslant -2.56\ \mathrm{eV}. \tag{11}$$

In the Te-rich condition $\Delta\mu_{\mathrm{Cd}} = E^f[\mathrm{CdTe}]$, then Eq. (9) becomes

$$\Delta\mu_{\mathrm{O}}^{\text{Te-rich}} \leqslant E^f[\mathrm{CdO}] - E^f[\mathrm{CdTe}] = -1.65\ \mathrm{eV}. \tag{12}$$

In this case, relation (8) is stricter. Hence,

$$\Delta\mu_{\mathrm{O}}^{\text{Te-rich}} \leqslant -1.88\ \mathrm{eV}. \tag{13}$$

D. DFT + *GW* formalism

The formation energy of a defect in charge state $q-1$ is given by

$$E_{q-1}^f[\mathbf{R}_{q-1}] = E_{q-1}[\mathbf{R}_{q-1}] - E_{\mathrm{ref}} + (q-1)E_F. \tag{14}$$

By adding and subtracting first $E_{q-1}[\mathbf{R}_q]$ and then $E_q[\mathbf{R}_q]$, we have

$$\begin{aligned} E^f_{q-1}[\mathbf{R}_{q-1}] &= \{E_{q-1}[\mathbf{R}_q] - E_q[\mathbf{R}_q]\} \\ &\quad +\{E_{q-1}[\mathbf{R}_{q-1}] - E_{q-1}[\mathbf{R}_q]\} \\ &\quad +E^f_q[\mathbf{R}_q] - E_F \\ &\equiv E_{\mathrm{QP}} + E_{\mathrm{relax}} + E^f_q[\mathbf{R}_q] - E_F. \end{aligned} \quad (15)$$

The first term, $E_{q-1}[\mathbf{R}_q] - E_q[\mathbf{R}_q]$, is a quasiparticle energy (E_{QP}) which is not accurately described within density functional theory. However, it may be evaluated by using the many-body perturbation theory based on the GW approximation [53,54]. The second term, $E_{q-1}[\mathbf{R}_{q-1}] - E_{q-1}[\mathbf{R}_q]$, corresponds to a relaxation energy (E_{relax}) and can be evaluated at DFT level, since we avoid the computation of energy differences between systems with different numbers of electrons.

Similarly,

$$\begin{aligned} E^f_{q+1}[\mathbf{R}_{q+1}] &= \{E_{q+1}[\mathbf{R}_q] - E_q[\mathbf{R}_q]\} \\ &\quad +\{E_{q+1}[\mathbf{R}_{q+1}] - E_{q+1}[\mathbf{R}_q]\} \\ &\quad +E^f_q[\mathbf{R}_q] + E_F \\ &\equiv E_{\mathrm{QP}} + E_{\mathrm{relax}} + E^f_q[\mathbf{R}_q] + E_F. \end{aligned} \quad (16)$$

By using the Kohn–Sham (KS) energy $\epsilon^{\mathrm{KS}}_{n,k}$ and wave function $\psi^{\mathrm{KS}}_{n,k}$, the quasiparticle energy is calculated by adding to $\epsilon^{\mathrm{KS}}_{n,k}$ the first-order perturbative correction

$$E^{\mathrm{QP}}_{n,k} = \epsilon^{\mathrm{KS}}_{n,k} + \langle \psi^{\mathrm{KS}}_{n,k} | \Sigma\big(E^{\mathrm{QP}}_{n,k}\big) - V_{\mathrm{xc}} | \psi^{\mathrm{KS}}_{n,k} \rangle, \quad (17)$$

which comes from replacing the KS exchange-correlation potential V_{xc} with the self-energy operator Σ. Because the exchange-correlation potential is less sensitive to the supercell size [55], quasiparticle corrections to the KS eigenvalues were obtained by using 64-atom supercells at the Γ point only. These corrections were then applied to the KS eigenvalues of 512-atom supercells to obtain the quasiparticle energies with respect to the averaged electrostatic potential of bulk CdTe. For the cases of ($\mathrm{Te_{Cd}}$) and ($\mathrm{O_{Te}}$-$\mathrm{Te_{Cd}}$), the finite-size error in the individual eigenvalues in the band gap was corrected by taking into account the position of the KS defect levels with respect to the VBM by using 64, 216, and 512 supercell sizes and extrapolating them to the dilute limit [48]. The relaxation energies where calculated by using 512-atom supercells.

E. Reference energy for DFT + GW scheme

As it is clearly shown in Eqs. (15) and (16), the DFT + GW formalism relies on the quality of at least one formation energy calculated within DFT. For the cases of $(\mathrm{O_{Te}})^0$, $(\mathrm{O_i})^0$, and $(\mathrm{O_{Cd}})^0$ the effects of the self-interaction and band-gap error on the formation energies should be small at DFT level, since they are ground-state configurations with all the valence bands full and all the conduction bands empty. We note that the self-interaction error, which artificially raises the VBM, will mostly cancel in the first difference of Eq. (1). Therefore, starting from $q = 0$, we obtain the formation energies for ($\mathrm{O_{Te}}$) and ($\mathrm{O_i}$) in different charge states by successive steps. Similarly, for ($\mathrm{O_{Te}}$-$\mathrm{Te_{Cd}}$) and ($\mathrm{O_{Te}}$-$\mathrm{V_{Cd}}$) we applied the DFT + GW scheme starting from the charge state +2 and −2, respectively.

TABLE I. Defect formation energies used as reference for the DFT + GW scheme. The Fermi energy is set to the valence-band maximum (all values are given in eV).

Reference system	E^f (Te rich)	E^f (Cd rich)
$(\mathrm{O_{Te}})^0$	1.33	1.12
$(\mathrm{O_{Te}}\text{-}\mathrm{Te_{Cd}})^{+2}$	0.66	2.27
$(\mathrm{O_{Cd}})^0$	2.79	4.40
$(\mathrm{O_i})^0$	1.57	2.27
$(\mathrm{O_{Te}}\text{-}\mathrm{V_{Cd}})^{-2}$	4.28	4.98

The formation energies obtained within DFT are shown in Table I.

III. RESULTS AND DISCUSSION

A. Isovalent oxygen ($\mathrm{O_{Te}}$)

Isovalent impurity systems are those in which the substitutional atoms have the same number of valence electrons as the host atoms they replace [56]. In most cases, isovalent doping does not produce a defect level inside the band gap, since the potential difference between the isovalent and the host atom is too small to confine a localized defect level. However, when chemical properties and size differences between the isovalent impurity and the substituted host atom are large, isovalent trap states may form [28,57–59].

The ground-state configuration of ($\mathrm{O_{Te}}$) has T_d symmetry. Oxygen is incorporated with full complement of the four-nearest-neighbor Cd atoms. The O–Cd bond length is found to be 2.13 Å. The formation energies of an isolated ($\mathrm{O_{Te}}$) are shown in Fig. 1. In line with previous studies [25,60], we find that ($\mathrm{O_{Te}}$) is an electrically neutral defect with formation energies of 1.33 eV in the Te-rich limit, and 1.12 eV in the Cd-rich limit.

Figure 2 shows the electronic band structure of ($\mathrm{O_{Te}}$) in the neutral charge state calculated by using a 512-atom cubic supercell. A scissors operator, consisting of a rigid shift to

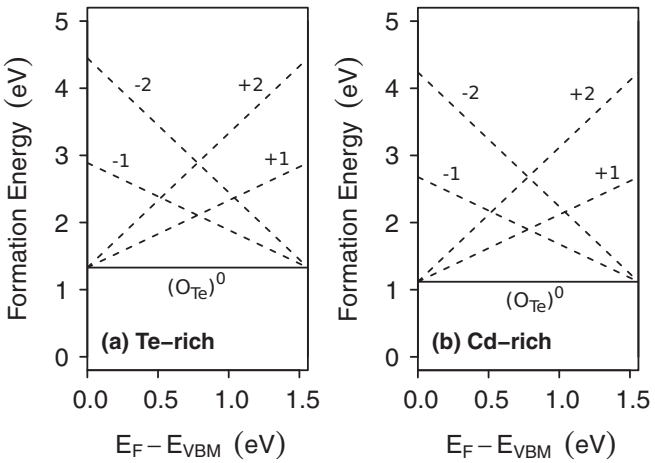

FIG. 1. Calculated formation energies of ($\mathrm{O_{Te}}$) in various charge states as a function of the Fermi level inside the band gap. The stable charge states are shown by solid lines.

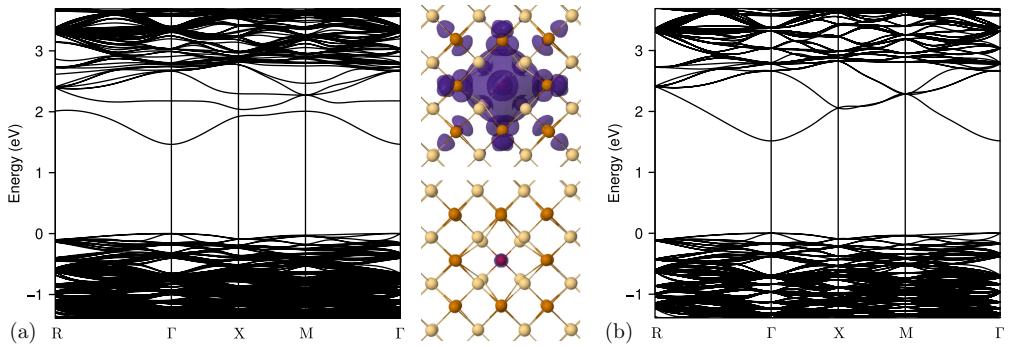

FIG. 2. (a) Calculated band structure of an isolated $(O_{Te})^0$ impurity and charge density isosurfaces ($\rho = 0.0003e/\text{Bohr}^3$) of the conduction-band edge (bottom right) and the impurity-induced state above the conduction-band edge (top right). (b) Electronic band structure of perfect CdTe. Electronic band structures were calculated by using 512-atom supercells.

the conduction bands so as to recover the G_0W_0 quasiparticle band gap, was applied to the KS band structure. The highly electronegative O atom introduces a resonant state above the conduction band edge. The charge density isosurface corresponding to this state shows the A_1 symmetry of the T_d point group, and that the wave function is strongly localized around the O atom and its first nearest neighbors [Fig. 2(a) (top right)]. The isosurface of the wave function corresponding to the conduction-band minimum (CBM) suggests that there is an interaction between this resonant state and the extended states of the conduction band [Fig. 2(a) (bottom right)]. Further insights about this interaction can be gained from the **k**-resolved projected density of states shown in Fig. 3. It reveals a strong hybridization between O 2*s* orbitals and the extended states of the conduction-band edge.

This phenomena can be described within the many-impurity Anderson model [61–63], resulting in the band anticrossing effect (BAC) [64,65] that describes the interaction of the extended band states of the host material with localized states introduced by the minority component of the alloy. A similar behavior has been recently reported for ZnSe:O [66].

B. (O_{Te}-Te_{Cd}) complex

Tellurium antisite (Te_{Cd}) has been proposed as a possible candidate to form a deep donor level, which is believed to be responsible for the pinning of the Fermi energy near the middle of the band gap in semi-insulating CdTe [16,67–69]. The ground-state structure of (Te_{Cd}) in the neutral charge state undergoes a Jahn–Teller distortion [69,70]. In T_d symmetry, electrons are localized at the high-symmetry anion site, leaving the localized electron manifold in a degenerate state. In this case, the Te antisite atom (i.e., the Te atom that substitutes a Cd atom) becomes a Jahn–Teller ion. A local site deformation to lower symmetry removes the orbital degeneracy at the cation. The Te antisite forms a plane with its three-nearest-neighboring Te atoms reducing the symmetry from T_d to C_{3v}. Figure 4(a) shows the electronic band structure of an isolated (Te_{Cd}) and the charge density isosurface of the deep energy level which appears 0.3 eV above the valence band maximum of CdTe. This nondegenerate isolated energy level may act as an effective nonradiative recombination center, degrading the performance of CdTe-based solar cells.

Recent theoretical and experimental studies indicate that oxygen exhibits a beneficial effect in CdTe. Korevaar *et al.* [71] found that CdTe films grown in 1 torr of oxygen show higher carrier lifetime and lower carrier density, achieving a better performance than devices without oxygen. Moreover, Feng *et al.* [72] found that oxygen prefers to segregate into Te-rich grain boundaries and substitute Te atoms with dangling bonds. Therefore, we investigate the possible role of oxygen in the passivation of deep energy levels associated with (Te_{Cd}).

The substitution of the Te atom far from the plane by an O atom reduces the anion-anion repulsion and antibonding

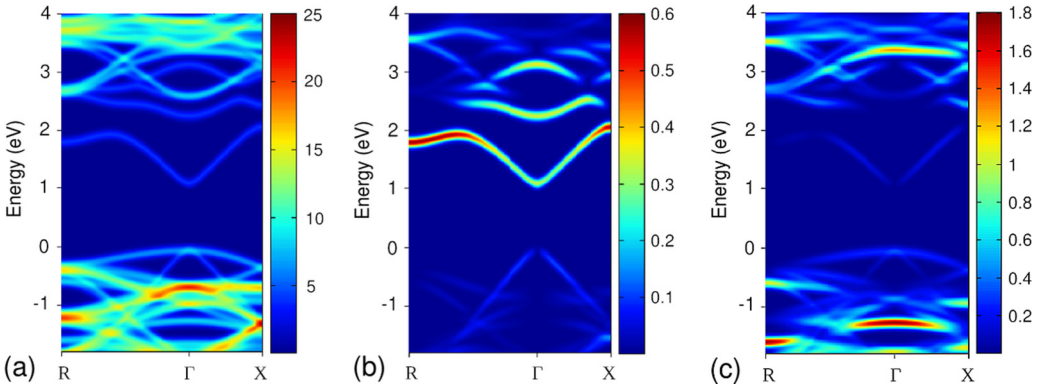

FIG. 3. (a) **k**-resolved total density of states of (O_{Te}), and **k**-resolved projected density of states of (b) O 2*s* and (c) O 2*p* atomic orbitals (in states/eV), calculated by using a 64-atom supercell.

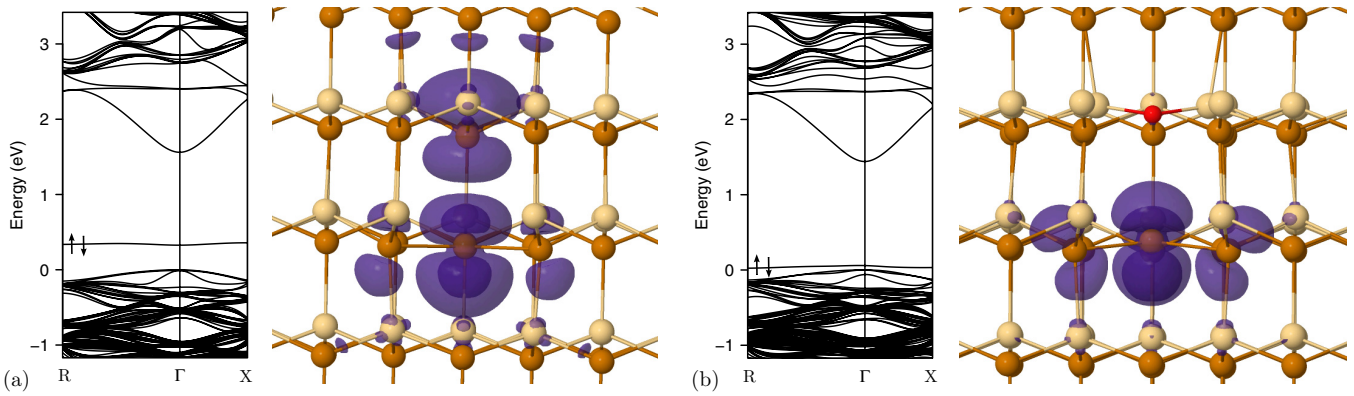

FIG. 4. Theoretical band structure and charge density isosurfaces ($\rho = 0.0005e/\text{Bohr}^3$) corresponding to the energy level in the band gap of (a) (Te_{Cd}) and (b) (O_{Te}-Te_{Cd}) in the neutral charge state calculated by using 216-atom supercells. A scissors operator, consisting of a shift of the defect level and a rigid shift of the conduction bands so as to recover the G_0W_0 quasiparticle band gap, was applied to the KS band structure. The arrows indicate the occupation of the energy level in the band gap. Dark spheres are Te atoms and light spheres are Cd atoms. In panel (b), the red sphere represents the oxygen impurity.

interaction between the former and the Te antisite atom, shifting the harmful deep energy level closer to the VBM. The oxygen impurity makes bonds with its three nearest neighbors without introducing dangling bonds. The Te antisite atom moves slightly along the C_{3v} threefold rotation axis up to a distance of 4.1 Å from the O atom, making an angle of 120° with its nearest-neighboring Te atoms. The theoretical band structure of (O_{Te}-Te_{Cd}) and the charge density isosurface of the localized energy level in the band gap are shown in Fig. 4(b). Because the anion-anion repulsion and antibonding interaction have been reduced, the energy level is now only separated 0.06 eV from the VBM. This small energy difference may be overcome by thermal energy, and thus trap-assisted carrier recombination is unlikely to occur.

Figure 5 shows the calculated formation energies for the (O_{Te}-Te_{Cd}) complex. In the Te-rich limit, its formation energy is found to be 0.85 eV in the neutral charge state, while the formation energy of an isoelectronic impurity (O_{Te}) is 1.33 eV. In the Cd-rich limit, the formation energy of (O_{Te}-Te_{Cd}) is 2.46 eV, higher than (O_{Te}). A (2+/0) transition level is found at the VBM + 0.09 eV.

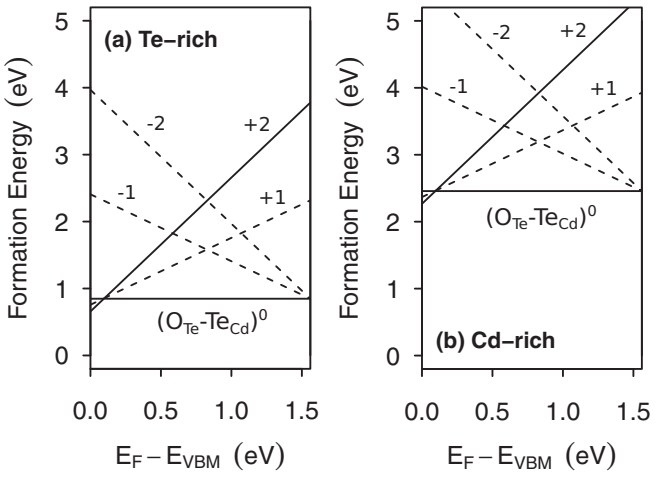

FIG. 5. Calculated formation energies of (O_{Te}-Te_{Cd}) in various charge states as a function of the Fermi level inside the band gap. The stable charge states are shown by the solid lines.

The contributions of each atomic orbital to the isolated energy level in the band gap of $(\text{Te}_{\text{Cd}})^0$ and $(\text{O}_{\text{Te}}\text{-}\text{Te}_{\text{Cd}})^0$ were assessed by **k**-resolved projected density of states calculations. According to our results, in $(\text{Te}_{\text{Cd}})^0$ the isolated state in the band gap contains a significant contribution from p orbitals of the Te antisite atom and from p orbitals of the other Te atom on the C_{3v} rotation axis. In the case of (O_{Te}-Te_{Cd}) a significant lattice relaxation occurs due to the smaller size of the O atom, which results in a reduction of the anion-anion repulsion and antibonding interaction. The main contribution to the defect level in the band gap comes from p orbitals of the Te antisite atom and p orbitals from its three-nearest-neighboring Te atoms.

C. Substitutional (O_{Cd})

The ground-state configuration of (O_{Cd}) has a C_{3v} local symmetry exhibiting a Jahn–Teller distortion similar to (Te_{Cd}). In T_d symmetry, there is a triple-degenerated energy level inside the band gap. A T_d-to-C_{3v} distortion removes the orbital degeneracy, leaving a fully occupied A_1^{a} level below the VBM and one empty E^{a} level resonant with the conduction bands. In the distorted configuration, the O atom forms a plane with its three-nearest-neighbor Te atoms with a bond length of 2.3 Å. The fourth Te atom is located along the C_{3v} threefold rotation axis at a distance of 3.58 Å from the O atom.

Figure 6 shows the formation energies of an isolated (O_{Cd}) in various charge states as a function of the Fermi level, in the Te- and Cd-rich-limit conditions. The only stable charge state of (O_{Cd}) is found to be neutral. Its formation energy is 2.79 eV in the Te-rich-limit condition, and 4.40 eV in the Cd-rich-limit condition. These high formation energies suggest that (O_{Cd}) is unlikely to form.

D. Interstitial oxygen (O_{i})

We investigate several atomic configurations for (O_{i}). The most stable structure is shown in Fig. 7(a). It is similar to the well-known off-bonding (Si–O–Si) interstitial in silicon

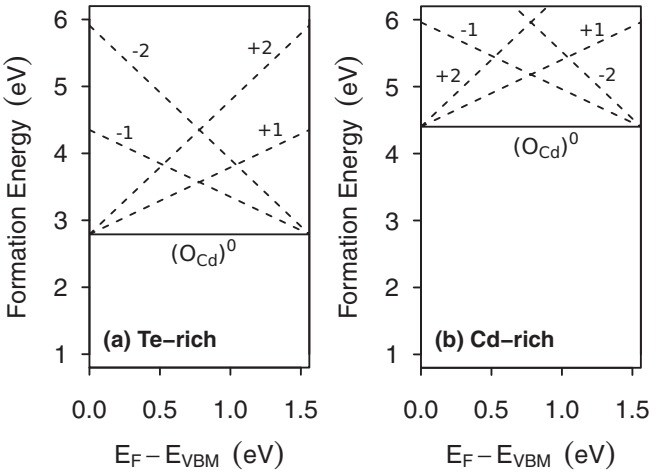

FIG. 6. Calculated formation energies of (O_{Cd}) in various charge states as a function of the Fermi level inside the band gap. The stable charge states are shown by the solid lines.

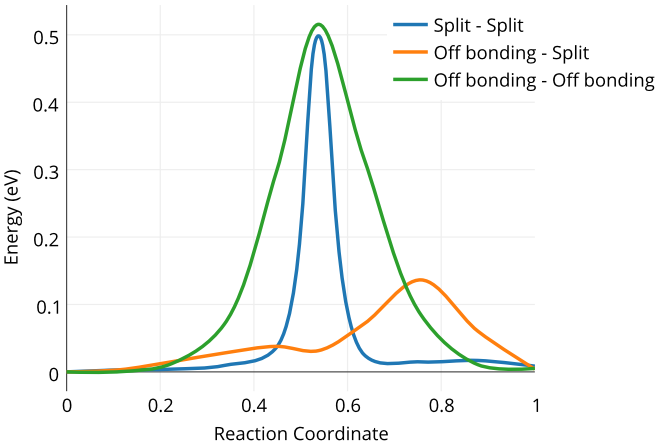

FIG. 8. Minimum-energy diffusion paths for oxygen between the most stable interstitial sites.

[73,74]. In the neutral charge state, Te-O and Cd-O bond lengths are 1.98 Å and 2.14 Å, respectively. We have also found another metastable configuration only 0.04 eV higher in energy, which forms a split interstitial $(Te\text{-}O)_{split}$ as is shown in Fig. 7(b). The Te-O_i bond length is 2.03 Å, and the bond lengths of the O atom with its neighboring Cd atoms in the split interstitial configuration are found to be 2.20 Å and 2.42 Å.

Having identified the lowest-energy interstitial sites, we now calculate the diffusion barriers between them. Figure 8 shows a comparison between the minimum-energy paths for (O_i) obtained from nudged elastic band (NEB) [75] calculations. We see immediately the existence a low energy barrier between split and off-bonding interstitial sites. The energy barrier between them is only 0.14 eV, much lower than all the other possible pathways. The energy barrier for the *off-bonding–off-bonding* and *split–split* interstitial sites is found to be 0.52 eV and 0.50 eV, respectively. It is worthwhile to mention that, in a recent calculation [76], the diffusion barrier between two O interstitials occupying a symmetric T_d site (tetrahedrally coordinated by Cd atoms) was found to be 1.51 eV. Our results indicate that this path is clearly unfavored.

The calculated formation energies of an isolated (O_i) impurity in various charge states are plotted as a function of the Fermi level in Fig. 9. The interstitial oxygen is found to be stable only in the neutral charge state. Therefore, (O_i) is an electrically neutral defect and does not introduce any electronic level in the band gap of CdTe. Its formation energy is calculated to be 1.57 eV in the Te-rich limit and 2.27 eV in the Cd-rich limit, in agreement with recent DFT calculations [77].

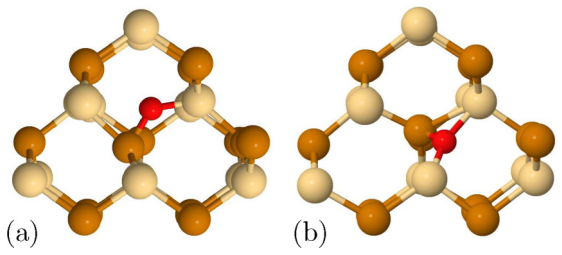

FIG. 7. Lowest-energy structures of (O_i) in the neutral charge state: (a) off-bonding configuration, (b) split configuration. Dark spheres are Te atoms and light spheres are Cd atoms. The red sphere represents the oxygen impurity.

E. (O_{Te}-V_{Cd}) complex

Next, we investigate the (O_{Te}-V_{Cd}) complex center. We find that this complex displays a C_{3v} local symmetry, in agreement with previous DFT calculations [25,78–80]. Oxygen replaces an isovalent Te anion in the vicinity of a Cd vacancy. The oxygen atom is bonded to its three Cd nearest neighbors with a bond length of 2.17 Å. Figure 10 shows the formation energies for the (O_{Te}-V_{Cd}) defect center in various charge states. It has a shallow acceptor level $\epsilon(-/2-)$ at the VBM + 0.05 eV, in good agreement with experimental observations [81].

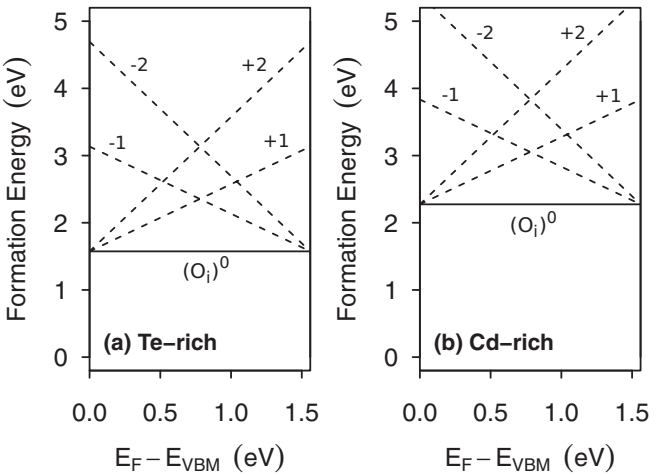

FIG. 9. Calculated formation energies of (O_i) in various charge states as a function of the Fermi level inside the band gap. The stable charge state is shown by the solid line.

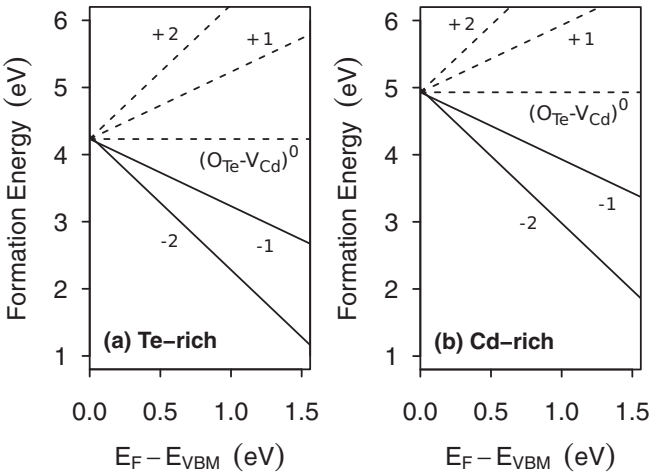

FIG. 10. Calculated formation energies of (O_{Te}-V_{Cd}) in various charge states as a function of the Fermi level inside the band gap. The stable charge states are shown by solid lines.

This complex was initially pointed out as responsible for the local vibrational modes (LVMs) observed by Chen *et al.* [78] via infrared spectroscopy. However, this assignment was later discarded by DFT calculations, which showed that the vibrational frequencies in the (O_{Te}-V_{Cd}) complex are significantly lower than the two modes observed experimentally [25,77]. Our results indicate that this complex has a high formation energy, higher than (O_{Te}), (O_{Te}-Te_{Cd}), and (O_i) in both Te-rich and Cd-rich conditions. Therefore, it is unlikely to form at a substantial concentration.

IV. SUMMARY

We investigated the formation energies, charge transition levels, and quasiparticle defect states of several oxygen-related impurities in CdTe within the DFT + *GW* formalism. Our calculations indicate that (O_{Te}) and (O_i) are electrically neutral defects with low formation energies. Isovalent oxygen adds an impurity state at the bottom of the conduction band, whereas substitutional (O_{Cd}) undergoes a Jahn–Teller distortion and is only stable in the neutral charge state.

In addition, we found a low-energy diffusion barrier for oxygen atoms of only 0.14 eV between two structurally distinct interstitial sites, one of them not previously reported. This low diffusion barrier suggests that oxygen can easily reach native defects to form complexes. One of these, the (O_{Te}-Te_{Cd}) complex, is energetically favored over both (O_{Te}) and (O_i) in the Te-rich condition. Furthermore, we find that (O_{Te}-Te_{Cd}) passivates the harmful deep energy levels derived from Te antisites, suggesting an explanation for the observed improvement in the efficiency of CdTe/CdS solar cells exposed to oxygen.

ACKNOWLEDGMENTS

This work was supported by the Fondo Nacional de Desarrollo Científico y Tecnológico (FONDECYT, Chile) under Grant No. 1130437. Powered@NLHPC: This research was partially supported by the supercomputing infrastructure of the NLHPC (ECM-02).

[1] B. Segall, M. R. Lorenz, and R. E. Halsted, Phys. Rev. **129**, 2471 (1963).
[2] G. M. Khattak and C. G. Scott, J. Phys.: Condens. Matter **3**, 8619 (1991).
[3] B. M. Basol, Sol. Cells **23**, 69 (1988).
[4] D. M. Hofmann, P. Omling, H. G. Grimmeiss, B. K. Meyer, K. W. Benz, and D. Sinerius, Phys. Rev. B **45**, 6247 (1992).
[5] X. Wu, Sol. Energy **77**, 803 (2004).
[6] C. Szeles, Phys. Status Solidi B **241**, 783 (2004).
[7] T. Schlesinger, J. Toney, H. Yoon, E. Lee, B. Brunett, L. Franks, and R. James, Mater. Sci. Eng., R **32**, 103 (2001).
[8] D. Kanzer, J. Phys. C: Solid State Phys. **6**, 2967 (1973).
[9] K. Biswas and M. Du, New J. Phys. **14**, 063020 (2012).
[10] A. Morales-Acevedo, Sol. Energy Mater. Sol. Cells **90**, 2213 (2006).
[11] C. Ferekides, U. Balasubramanian, R. Mamazza, V. Viswanathan, H. Zhao, and D. Morel, Sol. Energy **77**, 823 (2004).
[12] M. Gloeckler, I. Sankin, and Z. Zhao, IEEE J. Photovol. **3**, 1389 (2013).
[13] H. P. Mahabaduge, W. L. Rance, J. M. Burst, M. O. Reese, D. M. Meysing, C. A. Wolden, J. Li, J. D. Beach, T. A. Gessert, W. K. Metzger, S. Garner, and T. M. Barnes, Appl. Phys. Lett. **106**, 133501 (2015).
[14] K. Shen, Q. Li, D. Wang, R. Yang, Y. Deng, M.-J. Jeng, and D. Wang, Sol. Energy Mater. Sol. Cells **144**, 472 (2016).
[15] A. Shepidchenko, B. Sanyal, M. Klintenberg, and S. Mirbt, Sci. Rep. **5**, 14509 (2015).
[16] M. Fiederle, C. Eiche, M. Salk, R. Schwarz, K. W. Benz, W. Stadler, D. M. Hofmann, and B. K. Meyer, J. Appl. Phys. **84**, 6689 (1998).
[17] M. A. Berding, Phys. Rev. B **60**, 8943 (1999).
[18] O. Panchuk, A. Savitskiy, P. Fochuk, Y. Nykonyuk, O. Parfenyuk, L. Shcherbak, M. Ilashchuk, L. Yatsunyk, and P. Feychuk, J. Cryst. Growth **197**, 607 (1999).
[19] V. Babentsov, J. Franc, H. Elhadidy, A. Fauler, M. Fiederle, and R. James, J. Mater. Res. **22**, 3249 (2007).
[20] V. Babentsov, J. Franc, A. Fauler, M. Fiederle, and R. James, J. Mater. Res. **23**, 1751 (2008).
[21] N. Krsmanovic, K. G. Lynn, M. H. Weber, R. Tjossem, T. Gessmann, C. Szeles, E. E. Eissler, J. P. Flint, and H. L. Glass, Phys. Rev. B **62**, R16279 (2000).
[22] M. Chu, S. Terterian, D. Ting, C. C. Wang, H. K. Gurgenian, and S. Mesropian, Appl. Phys. Lett. **79**, 2728 (2001).
[23] M. Fiederle, A. Fauler, J. Konrath, V. Babentsov, J. Franc, and R. James, in *Proceedings of the IEEE 2003 Nuclear Science Symposium Conference Record* (IEEE, Portland, OR, 2003), Vol. 5, pp. 3478–3482.
[24] V. Babentsov, J. Franc, and R. James, Appl. Phys. Lett. **95**, 052102 (2009).
[25] M.-H. Du, H. Takenaka, and D. J. Singh, Phys. Rev. B **77**, 094122 (2008).

[26] V. Babentsov, V. Boiko, G. Schepelskii, R. James, J. Franc, J. Prochzka, and P. Hldek, J. Lumin. **130**, 1425 (2010).

[27] V. Babentsov, V. Boiko, G. Schepelskii, R. James, J. Franc, J. Prochzka, and P. Hldek, Nucl. Instrum. Methods Phys. Res., Sect. A **633**, S81 (2011).

[28] S. A. Awadalla, A. W. Hunt, K. G. Lynn, H. Glass, C. Szeles, and S.-H. Wei, Phys. Rev. B **69**, 075210 (2004).

[29] G. Contreras-Puente, O. Vigil-Galán, J. Vidal-Larramendi, F. Cruz-Gandarilla, M. Hesiquio-Garduño, J. Aguilar-Hernández, and A. Cruz-Orea, Thin Solid Films **387**, 50 (2001).

[30] C. Ding, Z. Ming, B. Li, L. Feng, and J. Wu, Mater. Sci. Eng., B **178**, 801 (2013).

[31] M. Emziane, K. Durose, D. P. Halliday, A. Bosio, and N. Romeo, J. Appl. Phys. **100**, 013513 (2006).

[32] V. Rejón, I. Riech, and J. L. Peña, Sol. Energy **95**, 319 (2013).

[33] N. Gorji, Opt. Quantum Electron. **47**, 2445 (2015).

[34] V. Valdna, Sol. Energy Mater. Sol. Cells **87**, 369 (2005).

[35] T. M. Hsu, R. J. Jih, P. C. Lin, H. Y. Ueng, Y. J. Hsu, and H. L. Hwang, J. Appl. Phys. **59**, 3607 (1986).

[36] M. Hedström, A. Schindlmayr, G. Schwarz, and M. Scheffler, Phys. Rev. Lett. **97**, 226401 (2006).

[37] P. Rinke, A. Janotti, M. Scheffler, and C. G. Van de Walle, Phys. Rev. Lett. **102**, 026402 (2009).

[38] A. Malashevich, M. Jain, and S. G. Louie, Phys. Rev. B **89**, 075205 (2014).

[39] J. P. Perdew, K. Burke, and M. Ernzerhof, Phys. Rev. Lett. **77**, 3865 (1996).

[40] P. Giannozzi *et al.*, J. Phys.: Condens. Matter **21**, 395502 (2009).

[41] K. F. Garrity, J. W. Bennett, K. M. Rabe, and D. Vanderbilt, Comput. Mater. Sci. **81**, 446 (2014).

[42] T. A. Pham, H.-V. Nguyen, D. Rocca, and G. Galli, Phys. Rev. B **87**, 155148 (2013).

[43] M. Govoni and G. Galli, J. Chem. Theory Comput. **11**, 2680 (2015).

[44] D. Rocca, R. Gebauer, Y. Saad, and S. Baroni, J. Chem. Phys. **128**, 154105 (2008).

[45] A. Grüneis, G. Kresse, Y. Hinuma, and F. Oba, Phys. Rev. Lett. **112**, 096401 (2014).

[46] D. Hamann, Phys. Rev. B **88**, 085117 (2013).

[47] L. Kleinman and D. M. Bylander, Phys. Rev. Lett. **48**, 1425 (1982).

[48] M. Jain, J. R. Chelikowsky, and S. G. Louie, Phys. Rev. Lett. **107**, 216803 (2011).

[49] C. G. Van de Walle and J. Neugebauer, J. Appl. Phys. **95**, 3851 (2004).

[50] *CRC Handbook of Chemistry and Physics*, 93rd ed., edited by W. M. Haynes (Taylor & Francis, Boca Raton, 2012).

[51] R. Diehl and B. I. Noläng, J. Cryst. Growth **66**, 91 (1984).

[52] V. Kräemer and G. Brandt, Acta Crystallogr., Sect. C: Cryst. Struct. Commun. **41**, 1152 (1985).

[53] L. Hedin, Phys. Rev. **139**, A796 (1965).

[54] M. S. Hybertsen and S. G. Louie, Phys. Rev. Lett. **55**, 1418 (1985).

[55] E.-A. Choi and K. J. Chang, Appl. Phys. Lett. **94**, 122901 (2009).

[56] R. A. Faulkner, Phys. Rev. **175**, 991 (1968).

[57] D. G. Thomas, J. J. Hopfield, and C. J. Frosch, Phys. Rev. Lett. **15**, 857 (1965).

[58] J. J. Hopfield, D. G. Thomas, and R. T. Lynch, Phys. Rev. Lett. **17**, 312 (1966).

[59] J. Li and S.-H. Wei, Phys. Rev. B **73**, 041201 (2006).

[60] S.-H. Wei and S. B. Zhang, Phys. Rev. B **66**, 155211 (2002).

[61] P. W. Anderson, Phys. Rev. **124**, 41 (1961).

[62] J. Wu, W. Walukiewicz, and E. E. Haller, Phys. Rev. B **65**, 233210 (2002).

[63] M. P. Vaughan and B. K. Ridley, Phys. Rev. B **75**, 195205 (2007).

[64] W. Walukiewicz, W. Shan, K. M. Yu, J. W. Ager, E. E. Haller, I. Miotkowski, M. J. Seong, H. Alawadhi, and A. K. Ramdas, Phys. Rev. Lett. **85**, 1552 (2000).

[65] J. Wu, W. Shan, and W. Walukiewicz, Semicond. Sci. Technol. **17**, 860 (2002).

[66] J.-H. Lee, J. Wu, and J. C. Grossman, Phys. Rev. Lett. **104**, 016602 (2010).

[67] M. Fiederle, V. Babentsov, J. Franc, A. Fauler, and J.-P. Konrath, Cryst. Res. Technol. **38**, 588 (2003).

[68] R. Grill, P. Fochuk, J. Franc, B. Nahlovskyy, P. Hschl, P. Moravec, Z. Zakharuk, Y. Nykonyuk, and O. Panchuk, Phys. Status Solidi B **243**, 787 (2006).

[69] A. Shepidchenko, S. Mirbt, B. Sanyal, A. Hkansson, and M. Klintenberg, J. Phys.: Condens. Matter **25**, 415801 (2013).

[70] J. Goodenough, Annu. Rev. Mater. Sci. **28**, 1 (1998).

[71] B. A. Korevaar, J. R. Cournoyer, O. Sulima, A. Yakimov, and J. N. Johnson, Prog. Photovol. **22**, 1040 (2014).

[72] C. Feng, W.-J. Yin, J. Nie, X. Zu, M. N. Huda, S.-H. Wei, M. M. Al-Jassim, and Y. Yan, Solid State Commun. **152**, 1744 (2012).

[73] S. Öberg, C. P. Ewels, R. Jones, T. Hallberg, J. L. Lindström, L. I. Murin, and P. B. Briddon, Phys. Rev. Lett. **81**, 2930 (1998).

[74] M. Pesola, J. von Boehm, and R. M. Nieminen, Phys. Rev. Lett. **82**, 4022 (1999).

[75] G. Mills and H. Jónsson, Phys. Rev. Lett. **72**, 1124 (1994).

[76] J. Roehl and S. Khare, Sol. Energy Mater. Sol. Cells **128**, 343 (2014).

[77] J. T-Thienprasert, T. Watcharatharapong, I. Fongkaew, M. H. Du, D. J. Singh, and S. Limpijumnong, J. Appl. Phys. **115**, 203511 (2014).

[78] G. Chen, I. Miotkowski, S. Rodriguez, and A. K. Ramdas, Phys. Rev. B **75**, 125204 (2007).

[79] J. T-Thienprasert, S. Limpijumnong, A. Janotti, C. V. de Walle, L. Zhang, M.-H. Du, and D. Singh, Comput. Mater. Sci. **49**, S242 (2010).

[80] E. V. Lavrov, D. Bastin, J. Weber, J. Schneider, A. Fauler, and M. Fiederle, Phys. Rev. B **84**, 233201 (2011).

[81] R. Soundararajan, K. Lynn, S. Awadallah, C. Szeles, and S.-H. Wei, J. Electron. Mater. **35**, 1333 (2006).